# MULTIPHYSICS IMPLEMENTATION OF ADVANCED SOIL MECHANICS MODELS

Navarro, V.[1], Asensio, L.[1], Alonso, J.[1], Yustres, Á.[1], Pintado, X.[2]

1. Geoenvironmental Group, Civil Engineering Department, University of Castilla-La Mancha, Spain

2. B+Tech Oy, Helsinki, Finland

*Authors' postprint version of the paper published in* Computers and Geotechnics:

Computers and Geotechnics 60 (2014) 20-28, doi:10.1016/j.compgeo.2014.03.012

## Abstract

Using multiphysics computer codes has become a useful tool to solve systems of partial differential equations. However, these codes do not always allow for the free introduction of implicitly defined state functions when automatic differentiation is used to compute the iteration matrix. This makes it considerably more difficult to solve geomechanical problems using non-linear constitutive models. This paper proposes a method for overcoming this difficulty based on multiphysics capabilities. The implementation of the well-known Barcelona basic model is described to illustrate the application of the method. For this purpose, without including formulation details addressed by other authors, the fundamentals of its implementation in a finite element code are described. Examples that demonstrate the scope of the proposed methodology are also presented.

## Keywords

Soil mechanics; Critical state model; Partial differential equations solver; Multiphysics environment; Automatic differentiation; Mixed method

## Abbreviations

| | |
|---|---|
| BBM | Barcelona Basic Model |
| CM | COMSOL Multiphysics |

| | |
|---|---|
| DODE | distributed ordinary differential equation |
| FEM | finite element method |
| MPDES | multiphysics partial differential equations solvers |
| PDE | partial differential equation |
| RRMSE | Relative Root Mean Square Error |

# 1. Introduction

In recent years, the application of numerical methods, particularly the finite element method (FEM), for solving boundary problems in soil mechanics has grown considerably, as illustrated by the high quality and large number of published papers on the subject. Among the noteworthy contributions to this area of research are those by Potts and Gens [1], Potts and Zdravkovic [2], Sheng et al. [3], Sheng et al. [4], Sheng et al. [5], Borja [6] and Gens and Potts [7]. The algorithms they propose have been implemented both in FEM codes developed primarily for research purposes [see 8,9 and 10] and in commercial FEM software [see, among others, 11–13], which include modules that facilitate the simulation of the behaviour of a large number of geotechnical structures (e.g., embankments and cuts, earth dams, retaining walls, slopes, tunnels and foundations).

The use of Multiphysics Partial Differential Equation Solvers (MPDES) emerges as a useful tool for the numerical solution of geotechnical problems [14]. With this class of solvers, the user defines the governing equations and models for the behaviour of the system. The code takes automatic control of assembling and solving the system of equations without it being necessary to redefine

the memory storage structures or to implement the algorithms for its solution. The user focuses on the physics of the problem, which allows for the coupling of almost any physical or chemical process that could be described through Partial Differential Equations (PDEs). This coupling ability is one of the main advantages of MPDES. In addition, some MPDES include specific stress–strain models for geomaterials in their libraries. For instance, COMSOL Multiphysics (CM) [15], the multiphysics partial differential equation solver used as a reference in this work, introduces a variety of saturated geomechanic material models (modified Cam-Clay, Matsuoka–Nakai, Hoek–Brown, among others).

Although built-in models are of great use, ideally users would be able to implement any desired stress–strain model. In principle, MPDES interfaces are adapted to so. Their structure enables to define different constitutive models. However, an important difficulty may arise when non-linear models are used. Several MPDES include automatic differentiation modules [16–19]. This method of evaluating derivatives has experienced a rapid advance, becoming an efficient tool in computing technology [20,21]. Some codes, as CM, differentiate symbolically all expressions that contribute to the iteration matrix [22]. In such case, if there are state functions defined through implicit relationships (as it happens in non-linear constitutive models), their derivatives cannot be calculated. Thus, the iteration matrix cannot be defined, and the program fails to solve the problem. Therefore, elastoplastic models cannot be freely implemented because they contain an implicit coupling between the stresses, plastic strains, and plastic variable increments. It is not possible either to implement simple models for non-linear elasticity, because both the volumetric and shear moduli are functions of stresses that must be calculated. This inability implies a very important limitation for the use of MPDES such as CM in the analysis of geomechanical boundary value problems.

This paper proposes a strategy for solving this problem using the multiphysics concept. A mixed method [see, for instance, 23] is proposed that identifies the stresses and plastic variables as main unknowns of the model. In this manner, users can freely introduce models with implicit couplings among the variables. To illustrate the application of the method, the Barcelona Basic Model (BBM) [24], a reference critical state model in unsaturated soil mechanics, has been implemented and analysed.

## 2. Formulation of the problem

To simplify the description of the methodology when analysing the mechanical behaviour of unsaturated soils, a soil consisting of three species, soil skeleton, water and air is considered in three phases: solid, liquid and gas. The presence of solids dissolved in the water is not considered, whereas the presence of dissolved air is considered according to Henry's law. The gas is formed by a mixture of dry

air and water vapour. The presence of vapour mixed with air in the gas phase is considered in accordance with the psychometric law. Because of this consideration, and assuming a displacement finite element approach, the solid displacements u, liquid pressure $P_L$ and gas pressure $P_G$ are the 'main unknowns' (state or primary variables) of the problem, and the mass balance of the species (soil, water and gas) and the equilibrium equation are the PDEs to solve. Isothermal conditions are assumed. Thus, no enthalpy balance is solved, and the temperature remains constant. The mass-balance equations implemented in the solver have been described in detail by Navarro and Alonso [9] and Alonso et al. [25].

The equilibrium equation is formulated in terms of the total stress tensor $\boldsymbol{\sigma}_{TOT}$ as follows:

(1) $$\nabla \cdot \boldsymbol{\sigma}_{TOT} + \rho \cdot g \cdot \mathbf{k} = \mathbf{0}$$

where '$\nabla\cdot$' is the divergence operator, $\rho$ is the average soil density, $g$ is the gravitational acceleration, and $\mathbf{k}$ is a unit vector in the direction of gravity. The total stress tensor $\boldsymbol{\sigma}_{TOT}$ is different from the constitutive stress $\boldsymbol{\sigma}$ used in the constitutive model. In this work, $\boldsymbol{\sigma}$ is assumed equal to the net stress ($\boldsymbol{\sigma} = \boldsymbol{\sigma}_{TOT} - P_G \cdot \mathbf{m}$, where $\mathbf{m}$ is the vector form of the Kronecker delta), and the mechanical behaviour of the soil is described by the pair of net stress and matric suction $s=P_G-P_L$ [26]. Thus, using the notation of Solowski and Gallipoli [27], the general constitutive relation is obtained as follows:

(2) $$d\boldsymbol{\sigma} = \mathbf{D}^{el} \cdot d\boldsymbol{\varepsilon}^{el,\sigma} = \mathbf{D}^{el} \cdot \left( d\boldsymbol{\varepsilon} - \left( d\boldsymbol{\varepsilon}^{pl} + d\boldsymbol{\varepsilon}^{el,s} \right) \right)$$

where $\mathbf{D}^{el}$ is the elastic matrix, and $d\boldsymbol{\varepsilon}^{el,\sigma}$ is the elastic strain associated with changes in the constitutive stresses. This latter term is the difference between the strain $d\boldsymbol{\varepsilon}$ (obtained by spatial differentiation of $\mathbf{u}$) and the sum of the plastic strain $d\boldsymbol{\varepsilon}^{pl}$ and elastic strain due to suction changes $d\boldsymbol{\varepsilon}^{el,s}$.

Introducing the definition for the plastic potential and the hardening law, the following relation is obtained [28]:

(3) $$d\boldsymbol{\sigma} = \mathbf{D}^{ep,\varepsilon} \cdot d\boldsymbol{\varepsilon} + \mathbf{D}^{ep,s} \cdot ds$$

where $\mathbf{D}^{ep,\varepsilon}$ is a 6×6 (three-dimensional problem) matrix defined as follows [27]:

$$\mathbf{D}^{ep,\varepsilon} = \mathbf{D}^{el} - \frac{\mathbf{D}^{el} \cdot \mathbf{g} \cdot \left(\frac{\partial F}{\partial \boldsymbol{\sigma}}\right)^{T} \cdot \mathbf{D}^{el}}{\left(\frac{\partial F}{\partial \boldsymbol{\sigma}}\right)^{T} \cdot \mathbf{D}^{e} \cdot \mathbf{g} - \frac{\partial F}{\partial p_{O}*} \frac{\partial p_{O}*}{\partial \varepsilon_{V}^{pl}} \mathbf{m}^{T} \cdot \mathbf{g}} \quad (4)$$

$\varepsilon_V^{pl}$ being the plastic volumetric strain, 'T' the transpose operator, and $F$ the yield function. $\mathbf{D}^{ep,s}$ is a 6×1 array defined as:

$$\mathbf{D}^{ep,s} = \mathbf{D}^{el} \cdot \left( \mathbf{g} \; \frac{\frac{\partial F}{\partial s} - \left(\frac{\partial F}{\partial \boldsymbol{\sigma}}\right)^{T} \cdot \mathbf{D}^{el} \cdot \mathbf{b}}{\left(\frac{\partial F}{\partial \boldsymbol{\sigma}}\right)^{T} \cdot \mathbf{D}^{el} \cdot \mathbf{g} - \frac{\partial F}{\partial p_{O}*} \frac{\partial p_{O}*}{\partial \varepsilon_{V}^{p}}} - \mathbf{b} \right) \quad (5)$$

where, if the BBM is used, the 6×1 array $\mathbf{b}$ is given by the expression [27]:

$$\mathbf{b} = \frac{1}{3} \frac{\kappa_{s}}{(P_{ATM} + s)(1+e)} \mathbf{m} \quad (6)$$

being $\kappa_s$ the elastic modulus for changes in suction, $P_{ATM}$ the atmospheric pressure (assumed to be 100 kPa), and $e$ the void ratio. As in other critical state models [29], the preconsolidation pressure $p_0$* in equations 4 and 2 is the model hardening parameter, defined in Fig. 1, where the 'hardening direction' $\mathbf{g}$ is also defined. For simplicity, in this work, $\mathbf{g}$ is taken as normal to $F$ in the $s$=constant plane, but it is simple to adapt the formulation to introduce a different flow rule. The variation of $p_0$* with respect to $\varepsilon_V^{pl}$ constitutes the hardening law, which is formulated according to the expression [27]:

$$dp_{O}* = \mathbf{H}^{\varepsilon} \cdot d\boldsymbol{\varepsilon} + H^{s} ds \quad (7)$$

where the vector $\mathbf{H}^{\varepsilon}$ (6×1) and scalar $H^{s}$ are defined as:

$$\mathbf{H}^{\varepsilon} = \frac{\partial p_{O}*}{\partial \varepsilon_{V}^{p}} \frac{\mathbf{m}^{T} \cdot \mathbf{g} \left(\frac{\partial F}{\partial \boldsymbol{\sigma}}\right)^{T} \cdot \mathbf{D}^{el}}{\left(\frac{\partial F}{\partial \boldsymbol{\sigma}}\right)^{T} \cdot \mathbf{D}^{el} \cdot \mathbf{g} - \frac{\partial F}{\partial p_{O}*} \frac{\partial p_{O}*}{\partial \varepsilon_{V}^{p}}} \quad (8)$$

(9) $$H^{s}=\frac{\partial p_{O}*}{\partial \varepsilon_{V}{}^{p}}\frac{\mathbf{m}^{T}\cdot\mathbf{g}\left(\frac{\partial F}{\partial s}-\left(\frac{\partial F}{\partial \boldsymbol{\sigma}}\right)^{T}\cdot\mathbf{D}^{el}\cdot\mathbf{b}\right)}{\left(\frac{\partial F}{\partial \boldsymbol{\sigma}}\right)^{T}\cdot\mathbf{D}^{el}\cdot\mathbf{g}-\frac{\partial F}{\partial p_{O}*}\frac{\partial p_{O}*}{\partial \varepsilon_{V}{}^{p}}}$$

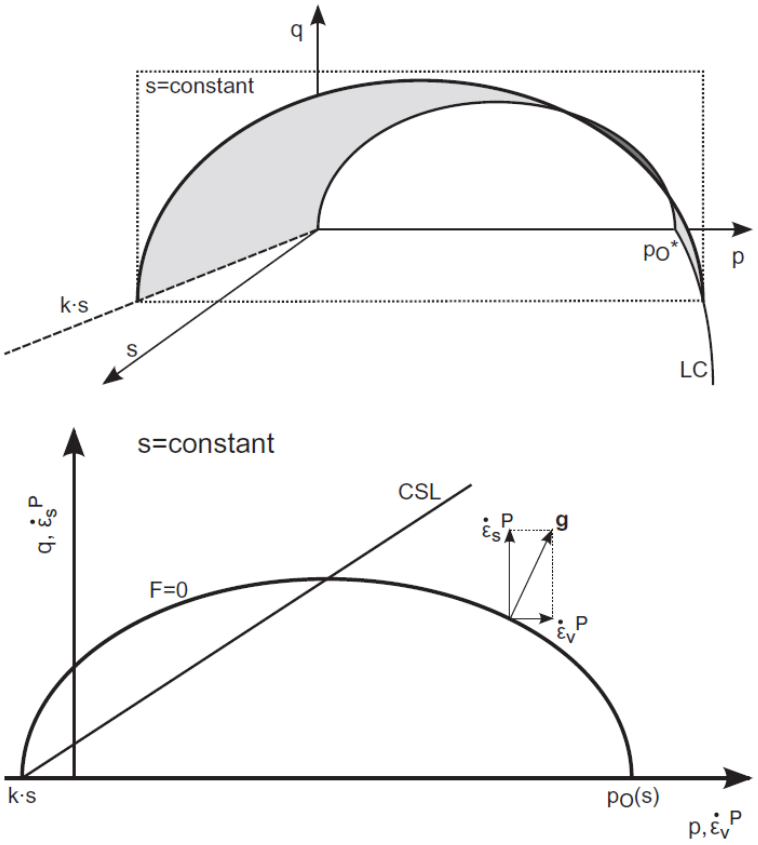


**Figure 1.** General form of the yield function. CSL is the Critical State Line

Therefore, if both a 'generalised' (or 'enhanced', in keeping with the notation of Solowski and Gallipoli [27]) strain vector $\boldsymbol{\varepsilon}_{enh}=(\boldsymbol{\varepsilon}, s)$, which includes strain and suction, and an 'enhanced' stress vector $\boldsymbol{\sigma}_{enh}=(\boldsymbol{\sigma}, p_O^*)$, which includes the constitutive stress and the hardening parameter, are defined, the following equation is obtained:

(10) $$d\boldsymbol{\sigma}_{enh}=(d\boldsymbol{\sigma}, dp_{O}*)=\begin{bmatrix}\mathbf{D}^{ep,\varepsilon} & \mathbf{D}^{ep,s}\\ \mathbf{H}^{\varepsilon} & H^{s}\end{bmatrix}\cdot\begin{bmatrix}d\boldsymbol{\varepsilon}\\ ds\end{bmatrix}=\mathbf{D}^{ep}{}_{enh}\cdot d\boldsymbol{\varepsilon}_{enh}$$

Consequently, using this notation and the proposed formulation, at each time step of the plastic path, the integration of Equation 10 is performed such that the increment $\delta\boldsymbol{\sigma}_{enh}=(\delta\boldsymbol{\sigma}, \delta p_0^*)$ satisfies the equation [1]:

(11) $$F\left(\boldsymbol{\sigma}+\delta\boldsymbol{\sigma},\, p_{\mathrm{O}}{}^{*}+\delta p_{\mathrm{O}}{}^{*},\, s+\delta s\right)=0$$

Sheng [30], Solowski and Gallipoli [27, 31] and Vaunat et al. [32] have described diverse strategies for solving this problem, focusing on their application to the BBM. Here, only yield by contact with the LC surface is considered [24] (see Fig. 1). Therefore, the problem is simplified considerably, with most of the difficulty focused on the selection of an explicit or implicit method [27].

However, as noted in the Introduction, the use of MPDES as CM involves other types of problems. The coefficients of $\mathbf{D}^{\mathrm{ep}}{}_{\mathrm{enh}}$ (see Equations 4 - 9 and Fig. 1) are functions of $\boldsymbol{\varepsilon}$ through the void ratio, as well as of $s$, $\boldsymbol{\sigma}$ and $p_0{}^{*}$. Therefore, the evolution of $\boldsymbol{\sigma}_{\mathrm{enh}}$ depends on the value of $\boldsymbol{\sigma}_{\mathrm{enh}}$. The use of elastoplastic models, in which the material behaviour is path dependent, introduces variables that are implicitly defined. If symbolic derivatives are computed, the program is not capable of managing this dependence. CM returns an error message and does not perform any calculation. This situation also occurs in the elastic regime if a non-linear elastic model is employed.

## 3. Solution strategy

The differentiation with respect to $\boldsymbol{\sigma}_{\mathrm{enh}}$ is needed to calculate $\mathbf{D}^{\mathrm{ep}}{}_{\mathrm{enh}}$. For that purpose, $\boldsymbol{\sigma}_{\mathrm{enh}}$ (vector grouping the state functions defined through implicit functions) can be identified as a new main unknown, so the logic of the computer algebra can differentiate with respect to it. Nevertheless, since new degrees of freedom are being introduced, new equations must be defined for them to be solved. Making use of the multiphysics capability of MPDES, a new balance equation can be defined:

(12) $$\frac{\partial\boldsymbol{\sigma}_{\mathrm{enh}}}{\partial t}-\mathbf{D}_{\mathrm{enh}}\cdot\frac{\partial\boldsymbol{\varepsilon}_{\mathrm{enh}}}{\partial t}+\nabla\cdot\mathbf{J}_{\sigma}=\mathbf{0}$$

If the 'stress flow' $\mathbf{J}_{\sigma}$ is restricted to zero, the fulfilment of Equation 12 is equivalent to the fulfilment of Equation 10. Consequently, when imposing $\mathbf{J}_{\sigma}\equiv\mathbf{0}$, Equation 12 defines an alternative way of introducing, through a PDE, the fulfilment of the initial value problem associated with Equation 10.

This strategy may be valid for any MPDES. In particular, regarding to CM, it is valid for any of its versions, even for the earlier ones. However, the latest versions of CM enable the direct definition of the initial value problem. The program includes the possibility of solving a distributed ordinary differential equation (DODE). This way, Equation 10 can be directly introduced as a DODE to obtain the equations that make the system independent.

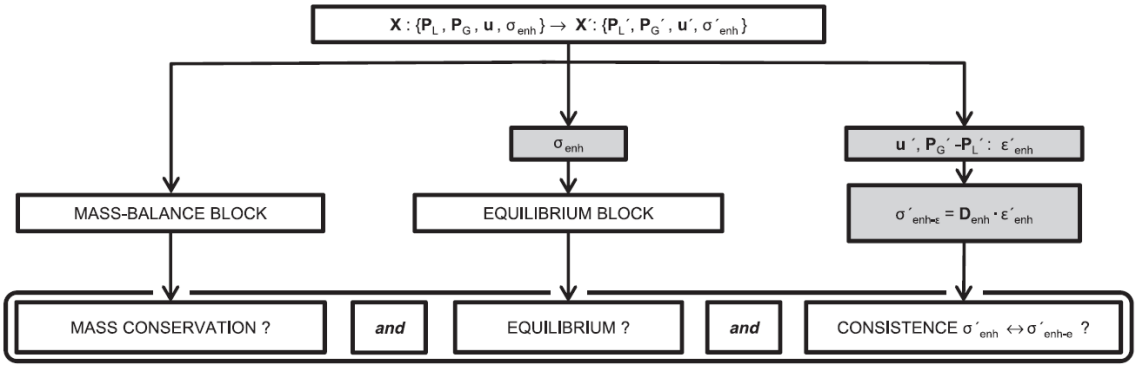


**Figure 2.** Scheme of the proposed calculation procedure

Regardless of whether Equation 12 with $\mathbf{J}_\sigma \equiv \mathbf{0}$ is used (general approach) or Equation 10 is introduced as a DODE in CM, it is important to note that the initial value problem defined is totally different from that obtained at each Gauss point when applying a classical displacement FEM. In such an approach, the solution to the initial value problem, defined by Equation 10, allows the enhanced stress to be obtained 'locally' [see, for instance, 33, 34] at each Gauss point and time step [27, 30-32]. However, when introducing Equation 12 with $\mathbf{J}_\sigma \equiv \mathbf{0}$, or Equation 10 implemented as a DODE, $\boldsymbol{\sigma}_{enh}$ is considered a main unknown. This way, a mixed method is being adopted [see, for example, 35], and as occurs with increments of displacements, liquid pressure and gas pressure (see Fig. 2), $\boldsymbol{\sigma}_{enh}$ should be determined in each node by solving the 'global' [33, 34] boundary value problem associated with each time increment.

To that end, the mass balance equations were solved as it is conventionally done in other FEM models [see, for example, 9 and 23]. In contrast, to solve the equilibrium equation, a non-conventional procedure was performed. In the weak formulation (application of the principle of virtual work, [36]) Equation 10 was not integrated to obtain the stress values in the Gauss points. Instead, the stress values included

in the vector $\mathbf{X}$ ($\equiv\{\mathbf{P}_L$ , $\mathbf{P}_G$, $\mathbf{u}$, $\boldsymbol{\sigma}_{enh}\}$), which defines the global unknowns of the system, were utilised (grey box in the centre of Fig. 2). Equation 10 as a DODE, or Equation 12 with $\mathbf{J}_\sigma \equiv \mathbf{0}$ as a PDE, ensure consistency among the values of $\boldsymbol{\sigma}_{enh}$ included in $\mathbf{X}$ and the values of $\boldsymbol{\varepsilon}_{enh}$ deduced from the values of $\mathbf{u}$, $P_L$ and $P_G$ that are also included in $\mathbf{X}$. By applying these equations, the calculation procedure indicated by the grey boxes located on the right side of Fig. 2 was followed. From the vector $\mathbf{X}'$ (time derivative of $\mathbf{X}$) the associated values of $\boldsymbol{\varepsilon}'_{enh}$ were obtained. With these values and $\mathbf{D}^{ep}{}_{enh}$, the conjugate value of the enhanced stress rate $\boldsymbol{\sigma}'_{enh\text{-}\varepsilon}$ was estimated. This value was compared with $\boldsymbol{\sigma}'_{enh}$ in $\mathbf{X}'$. Along with the residuals associated with the mass-balance and equilibrium equations, the difference $\boldsymbol{\sigma}'_{enh} - \boldsymbol{\sigma}'_{enh\text{-}\varepsilon}$ defines the residual vector $\mathbf{f}$. In each time step, the value of $\mathbf{X}$ (which includes $\boldsymbol{\sigma}_{enh}$) was determined globally such that $\mathbf{f}$ would be approximately zero.

## 4. Calculation procedure

As it was indicated in the Introduction, CM is the multiphysics partial differential equation solver used as a reference in this work, and it was used to carry out the validation exercises presented in the next section. Among the different options available in CM for the approximation of time derivatives, a fully implicit backward difference scheme was employed. The IDA module [37] developed by the Lawrence Livermore National Laboratory was used [see 38 and references therein]. In this module, the approximation order ranges from one (linear) to five, with the order $q$ differentiation formula given by the expression

$$\Delta_n t \cdot \mathbf{X}'_n = \sum_{i=0}^{q} \alpha_{n,i} \cdot \mathbf{X}_{n-i} \tag{13}$$

where $\mathbf{X}'_n$ and $\mathbf{X}_n$ are the computed approximations to $\mathbf{X}$ and its time derivative, respectively, at time n ($t_n$ ) and where $\Delta_n t$ is the n-th step size ($\Delta_n t = t_n - t_{n-1}$). The coefficients $\alpha_{n,i}$ are uniquely determinate by the order $q$ and the history of the step sizes. At the end of each time step, IDA analyses the convergence level attained and a new time step size and approximation order are automatically defined.

After the time discretisation, the resultant system $\mathbf{f}(\mathbf{X})=\mathbf{0}$ was solved via a damped Newton procedure. The procedure was described in detail by Deuflhard [39] and [37]. The iteration matrix was adopted equal to the system Jacobian, updated in each iteration of Newton's method. Each iteration was solved using the PARDISO solver [37, 40].

It is important to emphasise that, although the analytic computation of the Jacobian introduces the 'cost' of including additional variables (those in $\boldsymbol{\sigma}_{enh}$) in the global solving of the problem, it provides a very important calculation power. The 'true' Jacobian computed by using the automatic derivatives defined by the computer algebra preserves the quadratic rate of asymptotic convergence of the iterative solution. In addition, it is done automatically when modifying the physics of the analysis. If, for instance, the enthalpy flow or the consideration of transport of chemical species were introduced in the model, the derivatives of the terms included in the corresponding balance equations would be automatically calculated, keeping the convergence rate.

The iterative process is considered successfully solved when both the relative and the absolute errors are lower than user-defined tolerances [37]. When these conditions are not satisfied, the step size is reduced. The step size is also reduced when the iterative process reaches a maximum number of iterations. If the calculation step is not solved after a certain number of reductions in step size, the program stops the calculation process.

To conclude this section, it is interesting to point out that spatial discretisation in CM is accomplished by applying a FEM with Lagrange multipliers [41; see also 37, 42]. This point is important because this approach provides stability when applying a mixed method, as described by Babuška and Gatica [43]. Thus, such instabilities as those described by Cervera et al. [35] were not experienced in the analyses performed with this approach, even in the solution of complex problems, such as the deep geological storage of $CO_2$ in the supercritical phase [22, 44, 45], in which the propagation of a $CO_2$ front was analysed within a porous rock for which shear bands were produced with considerable strain localisation.

## 5. Validation exercises

As a validation exercise, various tests also simulated by Solowski and Gallipoli [31] have been analysed. Axisymmetric conditions were assumed. The enhanced strain increment vector has been defined in terms of strains invariants $\Delta\boldsymbol{\varepsilon}_{enh}=(\Delta\varepsilon_V, \Delta\varepsilon_S, \Delta s)$, where $\Delta\varepsilon_V$ is the increment of volumetric strain and $\Delta\varepsilon_s$ is the increment of shear strain. The net stress increment vector is defined in terms of triaxial stress states, i.e., in terms of the stress invariants ($\Delta p$, $\Delta q$).

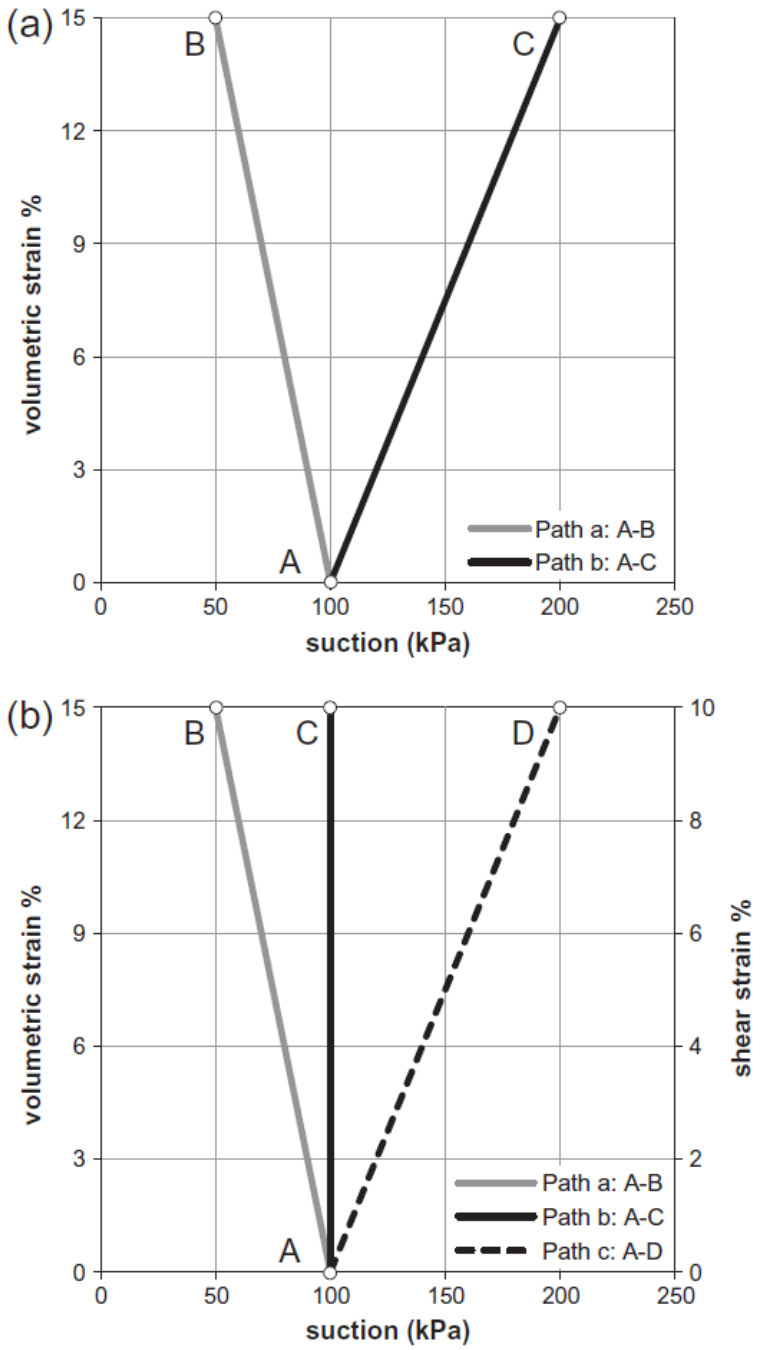


**Figure 3.** Deformation and suction paths of the validation exercises. (a) Exercise 1. (b) Exercise 2

In the first exercise, two isotropic compression paths ($\Delta\varepsilon_S \equiv 0$) under variable suction were simulated (see Fig. 3 a). In the second, three oedometric loading paths ($\Delta\varepsilon_S \equiv {}^2/_3 \cdot \Delta\varepsilon_V$) under variable suction were analysed (Fig. 3 b). The parameters in Table 1, taken from Solowski and Gallipoli [31, 46], were used in all analyses.

| $\lambda(0)$ | $\kappa$ | $r$ | $\beta$ (kPa$^{-1}$) | $pC$ (kPa) | $\kappa_s$ | $G$ (MPa) | $M$ | $k$ |
|---|---|---|---|---|---|---|---|---|
| 0.2 | 0.02 | 0.75 | 0.01 | 10 | 0.008 | 20 | 0.5 | 0.6 |

**Table 1.** Model parameters (adopted from [13, 48]).

A 'reference solution' (reference evolution of $p$, $q$ and $p_0$* upon varying $\varepsilon_V$, $\varepsilon_S$ and $s$) was obtained so that the solution attained with the proposed methodology could be validated against it. To do so, Equation 10 was integrated using an explicit Euler integration scheme. To run this calculation, a simple solver was programmed using the macro language Visual Basic for Applications of the Excel Spreadsheet (© Microsoft). The solution was considered accurate when the $p$ and $q$ values obtained with a twofold number of computation sub-increments differ by only $10^{-5}$ kPa. It has been proven that, in all of the analysed cases, these reference solutions are indistinguishable from the reference solutions adopted by Solowski and Gallipoli [31].

When carrying out the simulations with CM, equivalent boundary value problems were solved. The analysis of air mass balance was not activated, and it was assumed that the gas pressure is maintained at the atmospheric pressure. At any point in time, all points of the domain were allowed to have the value of $P_L$ deduced from the value of $s$. Consequently, the simulations carried out are a purely mechanical uncoupled analysis focused on the applicability of the proposed procedure.

A cylindrical 2-dimensional axisymmetric domain was used. It would have sufficed to use only a single linear finite element. However, to highlight the "global" character of the problem, and with the aim of preventing $\mathbf{X}$ from being reduced to $\boldsymbol{\sigma}_{enh}$ (see Fig. 2), a finite element mesh was analysed with four quadratic-

Lagrangian elements of rectangular shape. In this manner, the displacements of the internal nodes were also unknowns to be solved.

In the first validation (Fig. 3 a), an isotropic initial stress state corresponding to a mean net stress of 15 kPa and an initial value of the hardening parameter of 50 kPa were assumed. As can be observed in Fig. 4, the CM simulation overlaps with the reference solution.

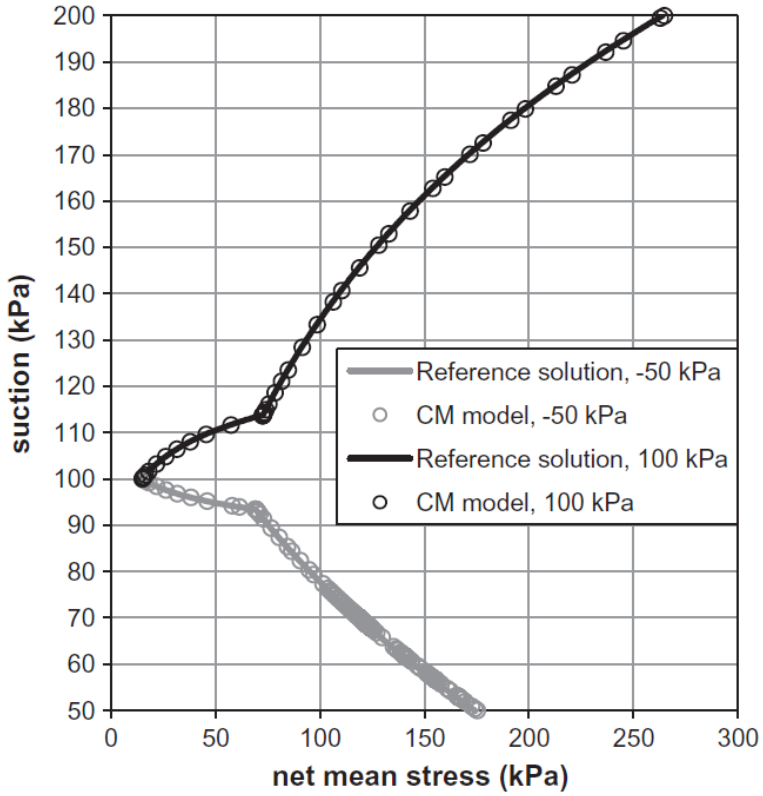


**Figure 4.** Validation exercise 1, Fig. 3a: Isotropic loading at variable suction

The CM solution also overlaps with the reference solution in the tests represented in Fig. 3 b, which corresponds to the second validation exercise. Three possible suction changes, -50, 0 and 100 kPa, were considered. The initial hardening parameter was assumed to be equal to 200 kPa. In the first test (Fig. 5 a), highly overconsolidated conditions were adopted, given that an initial mean net stress of 5 kPa was taken. In the second test (Fig. 5 b), the behaviour of a slightly overconsolidated soil was simulated, given that the initial mean stress was assumed to be equal to 200 kPa. In this test, the stress path yielded on the wet side of the plastic surface, whereas the yielding occurred on the dry side when starting from the highly overconsolidated condition. Therefore, with respect to Fig. 4

(isotropic path), Figs. 5 a and b indicate that the proposed procedure correctly simulates not only deviatoric paths but also paths on which hardening (Fig. 5 b, wet side) and softening occur (Fig. 5 a, dry side). The correct simulation of softening is always an important test for an elastoplastic model.

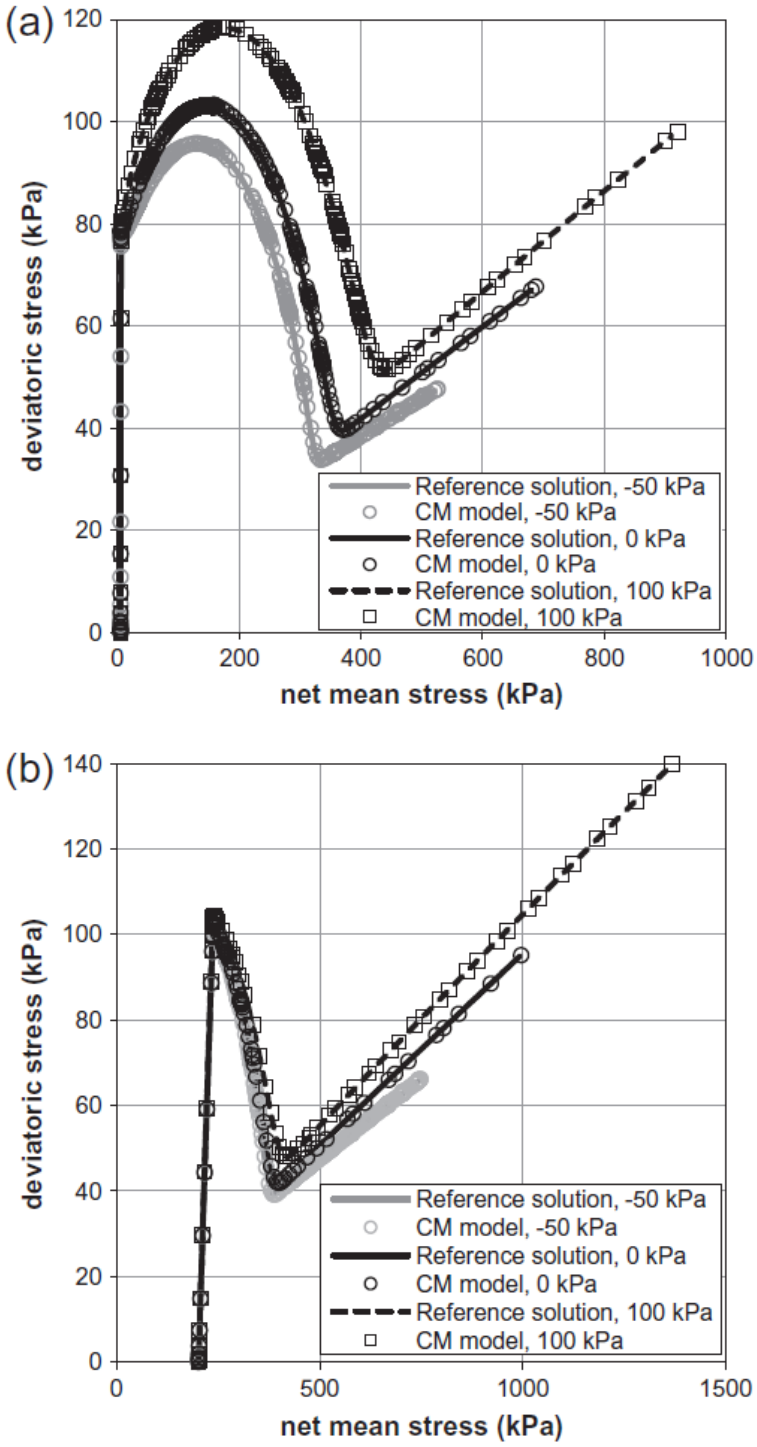


**Figure 5.** Validation exercise 2, Fig. 3b: Oedometric loading at variable suction. (a) Heavily overconsolidated soil. (b) Slightly overconsolidated soil.

To obtain a better comparison between the results obtained with CM and the reference solution, the 'distance' between both solutions was determined via the relative root mean square error (*RRMSE*), calculated as

$$RRMSE = \sqrt{\frac{1}{NCS}\sum_{i=1}^{NCS}\left(\frac{y_{CM} - y_R}{y_R}\right)^2} \quad (14)$$

where *NCS* is the number of computational steps used in the simulations with CM, $y_{CM}$ are the values obtained with CM, and $y_R$ are the values of the reference solution. In Fig. 4, the variable *y* corresponds to the values of the mean net stress, whereas in Figs. 5 a and b, *y* corresponds to the values of the deviatoric strain. The *RRMSE* values provided in Table 2 were obtained from the results depicted in Figs. 5 a and b. The table also includes an estimation of the best *RRMSE* values obtained by Solowski and Gallipoli [31] by utilising different integration methods. The results obtained with CM are comparable with those obtained by Solowski and Gallipoli [31].

| Test | $\Delta s$ (kPa) | Solowski and Gallipoli [12] | CM |
|---|---|---|---|
| Isotropic loading | -50 | 0.0034 | 0.0050 |
| | 100 | 0.0042 | 0.0046 |
| Oedometric loading. Heavily overconsolidated | -50 | 0.0470 | 0.0048 |
| | 0 | 0.0070 | 0.0032 |
| | 100 | 0.0048 | 0.0046 |
| Oedometric loading. Slightly overconsolidated | -50 | 0.0463 | 0.0027 |
| | 0 | 0.0044 | 0.0033 |
| | 100 | 0.0040 | 0.0031 |

**Table 2.** *RRMSE* associated with the simulations performed by Solowski and Gallipoli [13] and the simulations performed with CM.

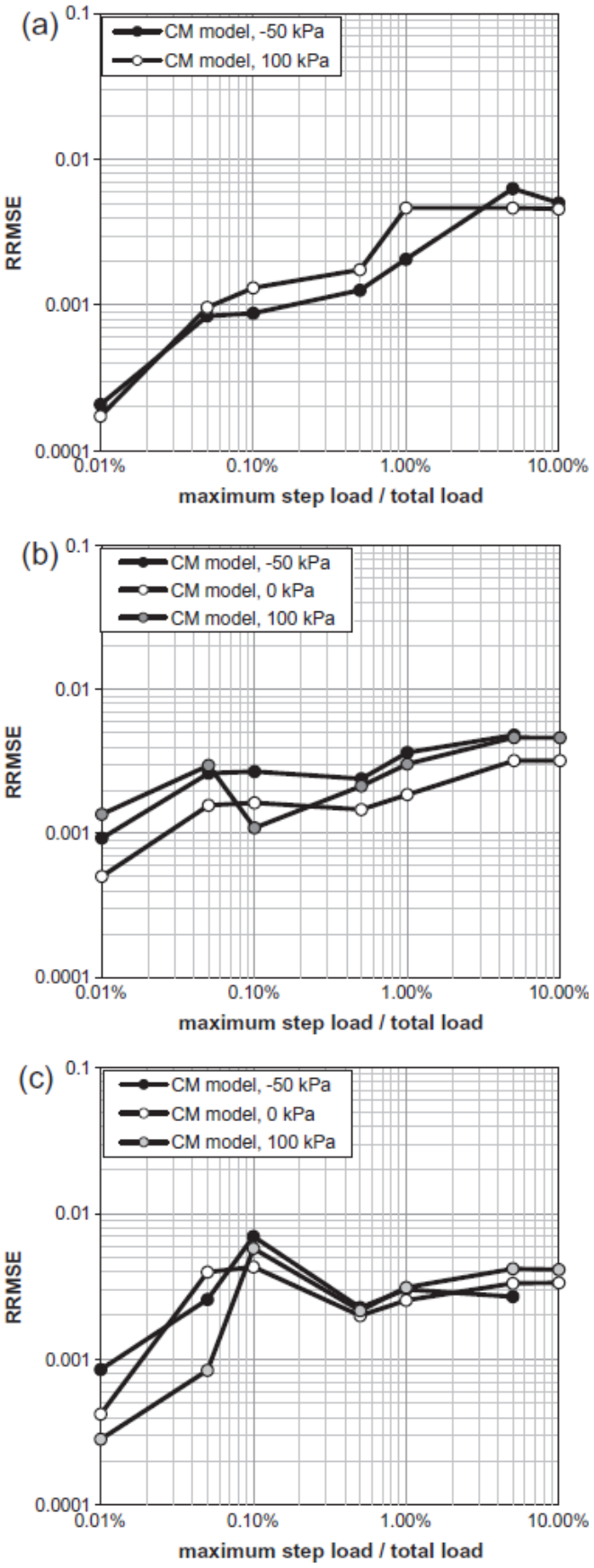


**Figure 6.** Variation of the RRMSE with the ratio 'maximum step load/total load'. (a) Isotropic loading. (b) Oedometric loading for heavily overconsolidated soil. (c) Oedometric loading for slightly overconsolidated soil.

The previous CM solutions were obtained with low computation requirements. First, a rather unrestrictive absolute tolerance of 0.1 kPa for $p$, $q$ and $p_0$*, and a relative tolerance of $10^{-3}$ were chosen. In addition, both the strain and the suction increments for each computational step were allowed to be up to 10% of the total increments defined in Figs. 3 a and b. Figures 6 a-c show the variation of *RRMSE* when reducing the ratio 'maximum step load / total load'. The variation of *RRMSE* is less than 0.48% when the reducing the mentioned ratio from 10 % to 0.01 %. It provides a quantitative estimate of the overall convergence quality of the proposed model.

This allows assuming that the steps adopted when modelling can be not necessarily of small size. This issue is of great importance to the proposed mixed formulation. By introducing $\boldsymbol{\sigma}_{enh}$ in $\mathbf{X}$, the number of unknowns $N$ in the system increases considerably. In accordance with Press et al. [47], the CPU consumption for a direct solver such as PARDISO [37, 40] can be approximated by $N^3$. Therefore, increasing $N$ implies significant increases in the computational cost. This increased cost is one of the main drawbacks of mixed methods [35]. Given that the cost of solving each time step will be greater with the proposed formulation, reducing the number of time steps without significantly reducing the quality of the solution is of great interest.

## 6. Coupled problems

When analysing coupled problems in which $P_L$ and $P_G$ are also main unknowns, the numerical performance is controlled not only by the mechanical problem, but also by the convergence of the mass balance. It will be of interest to know to what extent the use of the mixed formulation proposed herein modifies the number of time steps to solve. The general study of this question is beyond the scope of this research. However, an inspection exercise was performed by analysing a swelling pressure test.

The coupling between hydraulic and mechanical behaviour makes the swelling pressure test a valuable problem for this type of analysis. Therefore, a bentonite swelling pressure test was selected as an inspection example.

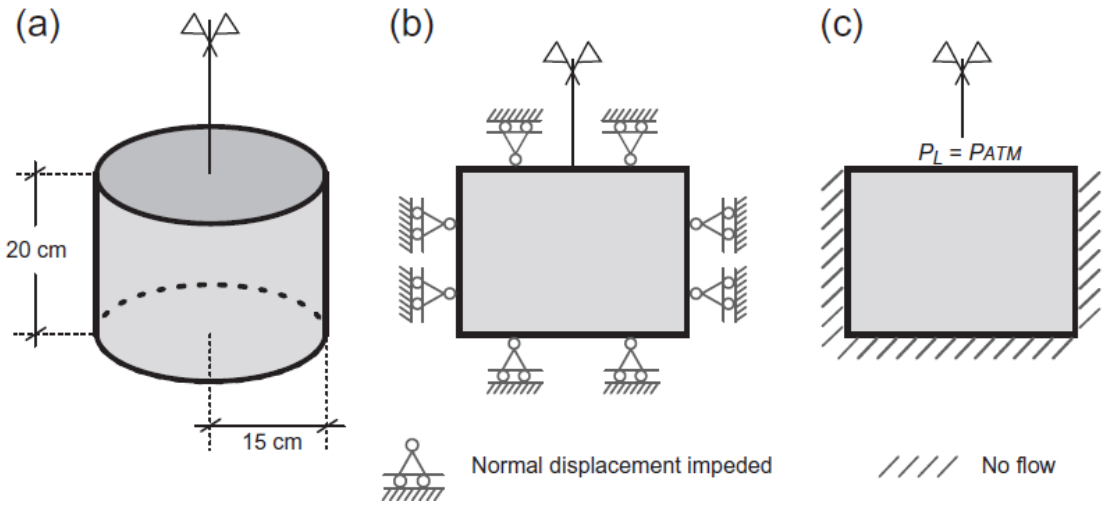


**Figure 7.** Configuration of the simulated swelling pressure test. (a) Test geometry. (b) Mechanical boundary conditions. (c) Hydraulic boundary conditions.

The saturation of a bentonite cylindrical sample with a radius of 15 cm and a height of 20 cm was simulated assuming axisymmetric conditions. A simple 16-element mesh was used. Quadratic Lagrangian elements of rectangular shape were adopted. Initially, the bentonite had a suction of 40 MPa (initial degree of saturation 60.2%), a void ratio of 0.68 and a dry density of 1.655 g/cm$^3$. It was subjected to a saturation boundary condition ($P_L$=$P_{ATM}$) applied at its top edge (vertical coordinate $z$=20 cm). Both vertical and radial deformations were restrained (see Fig. 7). A period of 11.6 days was simulated (minimum final degree of saturation equal to approximately one). The BBM was used as the mechanical constitutive model with the parameters listed in Table 3. A van Genuchten [48] retention curve was adopted, and the van Genuchten [48] – Mualem [49] formulation was assumed for the relative permeability. The intrinsic permeability $K$ in square meters was computed by using the formulation presented by Liu et al. [50]:

$$K = 10^{kk_1} \cdot \frac{n^{kk_2}}{(1-n)^{kk_3}} \quad (15)$$

where $n$ is the porosity, and $kk_1$, $kk_2$ and $kk_3$ are material parameters. The hydraulic parameters are provided in Table 4.

| | $\lambda(0)$ | $\kappa$ | $r$ | $\beta$ (MPa$^{-1}$) | $p_C$ (MPa) | $\kappa_s$ | $\nu$ | $M$ | $k$ | $p_0$* (MPa) |
|---|---|---|---|---|---|---|---|---|---|---|
| Elastic | - | 0.035 | - | - | - | 0.05 | 0.3 | - | - | - |
| Elastoplastic | 0.15 | 0.035 | 0.8 | $2 \cdot 10^{-2}$ | 0.01 | 0.05 | 0.3 | 1 | 0.1 | 5 |

**Table 3.** Bentonite mechanical parameters

| $\alpha$ (kPa$^{-1}$) [48] | $m$ [48] | $kk_1$ [50] | $kk_2$ [50] | $kk_3$ [50] |
|---|---|---|---|---|
| $3.74 \times 10^{-5}$ | 0.45 | -18 | 6 | 2 |

**Table 4.** Bentonite hydraulic parameters

Before solving the coupled problem, two uncoupled simulations were performed. In the first, which was only mechanical, an isotropic swelling pressure test $\varepsilon_V=\varepsilon_S=0$ with $\Delta s=-39.9$ MPa was simulated. The reference solution was compared with the CM solution to verify the quality of the mechanical solution. As shown in Fig. 8, the fit is similar to those shown in Figs. 4 and 5. In the simulations, a constant gas pressure equal to the atmospheric pressure was assumed. This hypothesis was also maintained when simulating water flow.

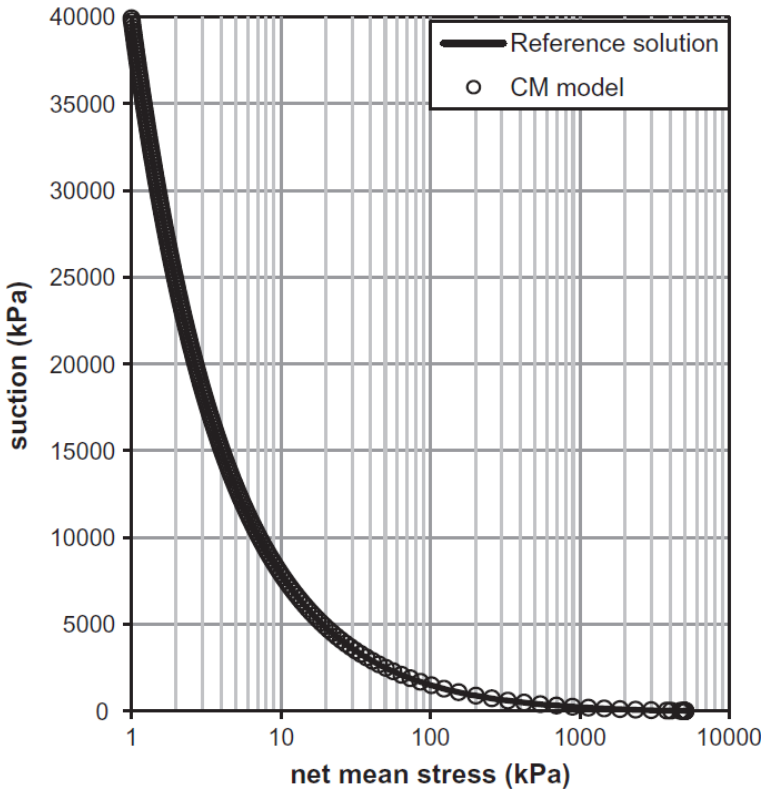


**Figure 8.** Isotropic swelling pressure test.

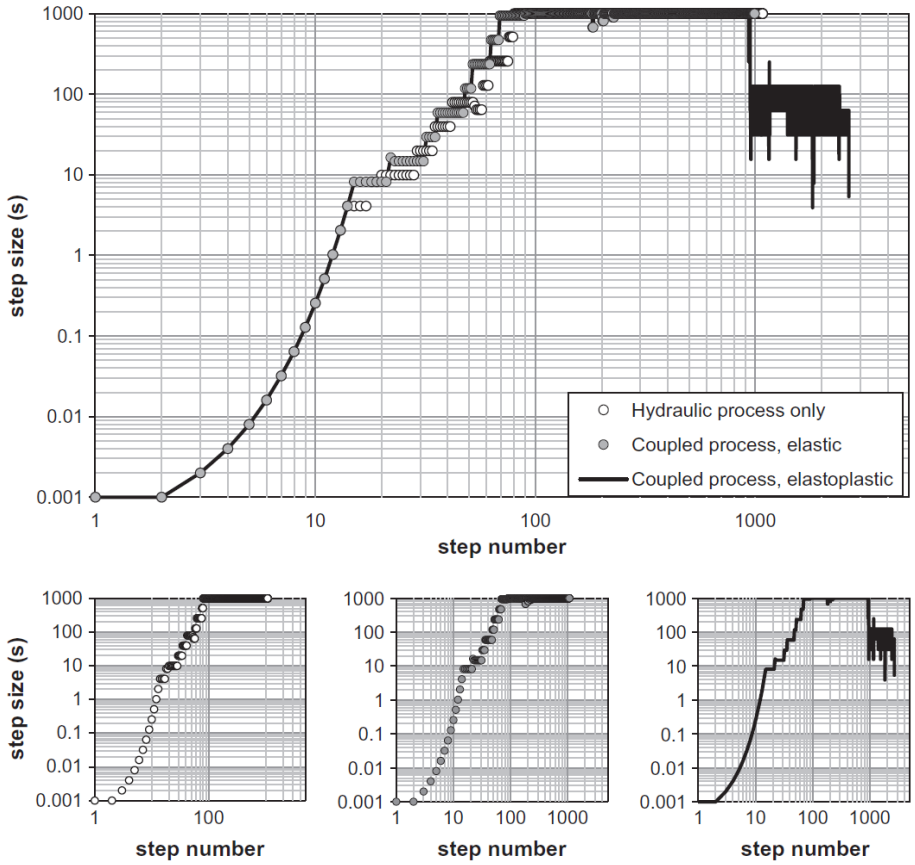


**Figure 9.** Number of time steps and step size when simulating the swelling pressure test. White dots, hydraulic process only. Grey dots, elastic coupled process. Black line, elastoplastic coupled process.

In the second uncoupled simulation, only the flow problem was analysed, assuming a non-deformable medium. As in the mechanical problem and coupled simulations, an absolute tolerance of 0.1 kPa was taken for $P_L$, equal to the one adopted for the stresses and $p_0$*. For all the state variables, the relative tolerance was equal to $10^{-3}$. The uncoupled resolution of the flow problem can be used as a reference of the numerical solution process, characterised by the number of time steps and their step size (Fig. 9). This reference was compared with the results obtained for a coupled simulation when assuming both a non-linear elastic mechanical behaviour and elastoplastic behaviour for bentonite (see the parameters in Table 3). As can be observed in Fig. 9, the elastic coupled solution is similar to that of the uncoupled flow problem in terms of time stepping. By having limited the maximum step size to 1000 s, the results of both simulations overlap when this maximum value has been reached. The coupled elastoplastic simulation has similar dynamics until the yield occurs (after the 947$^{th}$ time increment when

assuming an initial preconsolidation net stress of 5 MPa). From this point, the large demand of the plasticity calculation causes the calculation process to slow down. Thus, the numerical performance appears to be complicated not by the application of a mixed formulation but rather by the complexity of the stress-strain behaviour.

## 7. Conclusions

Although the analysis has been centred on the application of COMSOL Multiphysics (CM), it has been showed that the use of multiphysics capabilities enables the free implementation of advanced soil mechanic models, beyond built-in models, in Multiphysics Partial Differential Equation Solvers (MPDES) which use symbolic derivatives. The exercises performed here have focused on the well-known Barcelona basic model (BBM) [24]. However, the results are applicable to other elastoplastic models [25, 44].

The constitutive formulation, represented in Equation 10, is introduced, using the multiphysics capacity of MPDES, as a differential equation (Equation 12) assuming a zero 'stress flow', or as a distributed ordinary differential equation. Then, the constitutive stresses (net stresses in the adopted formulation) and preconsolidation pressure become main unknowns in the model. A mixed method was formulated (Fig. 2). Although these methods typically exhibit stability problems [35], the CM algorithmics (based on the application of the finite element method with Lagrange multipliers) and its computational stepping guarantee an efficient and accurate solution for the processes analysed. An important aspect of this efficiency is the automatic differentiation. It makes it possible to obtain derivatives defining a Jacobian that preserves the quadratic rate of the asymptotic convergence of the iterative solution scheme.

The performed validation exercises indicate that the results obtained with the proposed procedure are of comparable quality to those obtained by utilising integration methods typically employed in classical displacement finite element approaches (see Figs. 4, 5 and 8, and Table 2).

Notwithstanding, as occurs when mixed methods are used, the consideration of stresses and the plastic parameters as main unknowns implies a marked increase

in computational cost. A loss of 'computational efficiency' will occur. Future studies should determine whether this loss is compensated by the gain in 'conceptual efficiency' implied by having advanced geomechanical models (BBM is a good example) implemented in a multiphysics environment. In problems with well-defined physics, the loss might be greater than the gain. However, the same will not occur in the analysis of problems for which it is important to be able to activate (or deactivate) new physics with agility in the conceptual model of the system.

## Acknowledgements

This research was financed in part by B+TECH Oy under a POSIVA Oy project (Finland) and the FPU Grant AP2009-2134 of the Spanish Ministry of Education awarded to Ms Asensio. In addition, the financial support provided by the Spanish Ministry of Economy and Competitiveness in the frame of Innocampus Program 2010 is gratefully acknowledged.

## References

[1] Potts DM, Gens A. A critical assessment of methods of correcting for drift from the yield surface in elasto-plastic finite-element analysis. Int J Numer Anal Meth Geomech 1985;9(2):149–59.

[2] Potts DM, Zdravkovic L. Finite element analysis in geotechnical engineering: theory. London: Thomas Telford; 1999.

[3] Sheng D, Sloan SW, Yu HS. Aspects of finite element implementation of critical state models. Comput Mech 2000;26(2):185–96.

[4] Sheng D, Sloan SW, Gens A, Smith DW. Finite element formulation and algorithms for unsaturated soils. Part 1: Theory. Int J Numer Anal Meth Geomech 2003;27(9):745–65.

[5] Sheng D, Gens A, Fredlund DG, Sloan SW. Unsaturated soils: from constitutive modelling to numerical algorithms. Comput Geotech 2008;35(6):810–24.

[6] Borja RI. Cam-Clay plasticity. Part V: A mathematical framework for threephase deformation and strain localization analyses of partially saturated porous media. Comput Method Appl Mech Eng 2004;193(48–51):5301–38.

[7] Gens A, Potts DM. Critical state models in computational geomechanics. Eng Comput 1988;5(3):178–97.

[8] Olivella S, Gens A, Carrera J, Alonso EE. Numerical formulation for a simulator (CODE_BRIGHT) for the coupled analysis of saline media. Eng Comput 1996;13(7):87–112.

[9] Navarro V, Alonso EE. Modeling swelling soils for disposal barriers. Comput Geotech 2000;27(1):19–43.

[10] Thomas HR, Ferguson WJ. A fully coupled heat and mass transfer model incorporating contaminant gas transfer in an unsaturated porous medium. Comput and Geotech 1999;24(1):65–87.

[11] ABAQUS TM. Version 6.8. Hibbit, Karlsson and Sorensen Inc.; 2008.

[12] Brinkgreve RBJ, Broere W, Waterman D. PLAXIS 2D version 9.0: Material Models Manual; 2008.

[13] ANSYS Inc., Users Guide Documentation, version 12.0. Southpointe; 2011.

[14] Keyes DE, McInnes LC, Woodward C, Gropp W, Myra E, Pernice M, et al. Multiphysics simulations: challenges and opportunities. Int J High Perform Comput Appl 2013;27(1):4–83. http://dx.doi.org/10.1177/1094342012468181.

[15] COMSOL AB. Geomechanics Module User's Guide, version 4.2. 2011.

[16] Pawlowski R, Bartlett R, Belcourt N, Hooper R, Schmidt R. A theory manual for multi-physics code coupling in LIME, version 1.0. Sandia Report SAND 2011–2195. Sandia National Laboratories; 2011.

[17] Palacios F, Colonno MR, Aranake AC, Campos A, Copeland SR, Economon TD, et al. Stanford University Unstructured (SU2): an open-source integrated computational environment for multiphysics simulation and design. AIAA Paper 2013–0287, 51st AIAA Aerospace Sciences Meeting and Exhibit. January 7–10, Grapevine, Texas; 2013. doi:10.2514/6.2013-287.

[18] Bischof CH, Hovland PD, Norris B. On the implementation of automatic differentiation tools. Higher-Order Symb Comput 2008;21(3):311–31.

[19] Martins JRRA, Hwang JT. Review and unification of methods for computing derivatives of multidisciplinary systems. AIAA Paper 2012–1589. In: 53rd AIAA/ASME/ASCE/AHS/ASC structures, structural dynamics and materials conference. Honolulu, Hawaii; 2012.

[20] Corliss G, Faure C, Griewank A, Hascoet L, Naumann U, editors. Automatic differentiation of algorithms: from simulation to optimization. Springer; 2002.

[21] Griewank A, Walther A. Evaluating derivatives: principles and techniques of algorithmic differentiation. 2nd ed. Philadelphia: Society for Industrial and Applied Mathematic; 2008.

[22] Gobbert MK, Churchill A, Wang G, Seidman TI. COMSOL Multiphysics for efficient solution of a transient reaction-diffusion system with fast reaction. In: Rao Y, editor. Proceedings of the COMSOL Conference 2009, Boston; 2009.

[23] Malkus DS, Hughes TJR. Mixed finite-element methods – reduced and selective integration techniques: unification of concepts. Comput Method Appl Mech Eng 1978;15(1):63–81.

[24] Alonso EE, Gens A, Josa A. A constitutive model for partially saturated soils. Géotechnique 1990;40(3):405–30.

[25] Alonso J, Navarro V, Calvo B. Flow path development in different CO2 storage reservoir scenarios. A critical state approach. Eng Geol 2012;127:54–64. http://dx.doi.org/10.1016/j.enggeo.2012.01.001.

[26] Houlsby GT. The work input to an unsaturated granular material. Géotechnique 1997;47(1):193–6.

[27] Solowski WT, Gallipoli D. Explicit stress integration with error control for the Barcelona Basic Model. Part 1: Algorithms formulations. Comput Geotech 2010;37(1–2):59–67.

[28] Ledesma A, Chan AHC, Vaunat J, Gens A. Finite element formulation of an elasto-plastic model for partially saturated soils. In: Owen DRJ, Oñate E, editors. Computational plasticity: fundamentals and applications: proceedings of the fourth international conference. Pineridge Press; 1995. p. 1677–88.

[29] Roscoe KH, Burland J. On the generalized stress–strain behaviour of 'wet' clay. In: Heyman FLJ, editor. Engineering Plasticity. Cambridge: Cambridge University Press; 1968. p. 535–609.

[30] Sheng D. Review of fundamental principles in modelling unsaturated soil behaviour. Comput Geotech 2011;38(6):757–76.

[31] Solowski WT, Gallipoli D. Explicit stress integration with error control for the Barcelona Basic Model. Part 2: Algorithms efficiency and accuracy. Comput Geotech 2010;37(1–2):68–81.

[32] Vaunat J, Cante JC, Ledesma A, Gens A. A stress point algorithm for an elastoplastic model in unsaturated soils. Int J Plast 2000;16(2):121–41.

[33] Crisfield MA. Non-linear finite element analysis of solids and structures. Essentials, vol. 1. Chichester: John Wiley & Sons; 1991.

[34] Crisfield MA. Non-linear finite element analysis of solids and structures. Advanced topics, vol. 2. Chichester: John Wiley & Sons; 1997.

[35] Cervera M, Chiumenti M, Codina R. Mixed stabilized finite element methods in nonlinear solid mechanics Part I: Formulation. Comput Method Appl Mech Eng 2010;199(37–40):2559–70.

[36] Zienkiewicz OC, Taylor RL, Zhu JZ. The finite element method: its basis and fundamentals. 6th ed. Elsevier; 2005.

[37] COMSOL AB. COMSOL Multiphysics Reference Guide, version 4.2; 2011.

[38] Hindmarsh AC, Brown PN, Grant KE, Lee SL, Serban R, Shumaker DE, et al. SUNDIALS: suite of nonlinear and differential/algebraic equation solvers. ACM Trans Math Softw 2005;31(3):363–96.

[39] Deuflhard P. A modified Newton method for the solution of ill-conditioned systems of nonlinear equations with application to multiple shooting. Numer Math 1974;22(4):289–315.

[40] Schenk O, Gartner K. Solving unsymmetric sparse systems of linear equations with PARDISO. Future Gener Comput Syst 2004;20(3):475–87.

[41] Babuška I. The finite element method with Lagrangian multipliers. Numer Math 1973;20(3):179–92.

[42] COMSOL AB. COMSOL Multiphysics Modeling Guide, version 3.5a; 2008.

[43] Babuška I, Gatica GN. On the mixed finite element method with Lagrange multipliers. Numer Meth Part Differ Equat 2003;19(2):192–210.

[44] Alonso J, Navarro V, Calvo B, Asensio L. Hydro-mechanical analysis of CO2 storage in porous rocks using a critical state model. Int J Rock Mech Min Sci 2012;54:19–26. http://dx.doi.org/10.1016/j.ijrmms.2012.05.016.

[45] Navarro V, Alonso J, Calvo B, Sanchez J. A constitutive model for porous rock including effects of bond strength degradation and partial saturation. Int J Rock Mech Mining Sci 2010;47(8):1330–8. http://dx.doi.org/10.1016/j.ijrmms.2010.08.003.

[46] Solowski WT, Gallipoli D. A stress–strain integration algorithm for unsaturated soil elastoplasticity with automatic error control. In: Schweiger HF, editor. Numerical methods in geotechnical engineering – proceedings of the 6th European Conference on Numerical Methods in Geotechnical Engineering. Graz: Taylor & Francis Group; 2006. p. 113–9.

[47] Press WH, Teukolsky SA, Vetterling WT, Flannery BP, editors. Fortran Numerical Recipes, vol. 1. Numerical Recipes in Fortran 77: The Art of Scientific Computing. Cambridge: Cambridge University Press; 1992.

[48] Van Genuchten MT. A closed-form equation for predicting the hydraulic conductivity of unsaturated soils. Soil Sci Soc Am J 1980;44:892–8.

[49] Mualem Y. A new model for predicting the hydraulic conductivity of unsaturated porous media. Water Resour Res 1976;12:513–22.

[50] Liu L, Neretnieks I, Moreno L. Permeability and expansibility of natural bentonite MX-80 in distilled water. Phys Chem Earth 2011;36(17–18):1783–91.